PERGAMON

International Journal of Heat and Mass Transfer 42 (1999) 2883–2895

International Journal of HEAT and MASS TRANSFER

Conjugate heat transfer during two-phase solidification process in a continuously moving metal using average heat capacity method

M. Ruhul Amin*, David Greif

Department of Mechanical & Industrial Engineering, Montana State University, Bozeman, MT 59717, U.S.A.

Received 1 June 1998; in final form 6 October 1998

Abstract

The average heat capacity method was successfully implemented for the analysis of conjugate heat transfer during the two-phase solidification process in continuous castings. The finite element technique with fixed grid was used for the current research. This method overcomes the limitation of the time increment of the otherwise so-called effective heat capacity method. The investigation included the ranges of mold cooling rate (Bi_2), post-mold cooling rate (Bi_3), superheat (Θ_o), and withdrawal speed (Pe) from 0.025 to 0.075, 0.042 to 0.126, 1.2 to 2.7, and 1.0 to 3.45, respectively. The current study shows that two parameters, namely, Pe and Θ_o are very important in controlling the microstructure and breakout condition of the cast material.

Nomenclature

Bi Biot number, hW/k
C_p specific heat
g gravitational acceleration
h convective heat transfer coefficient
H height of the cast material, see Fig. 1
h_r radiation heat transfer coefficient
k thermal conductivity
L latent heat
P pressure
Pe Peclet number, U_oW/α_s
Q dimensionless average heat flux, equation (10)
q'' dimensional local heat flux
$q^{*''}$ dimensionless local heat flux, equation (9)
Ste Stefan number, $C_s(T_f-T_\infty)/L$
t time
T temperature
u x-component of velocity
U_o withdrawal speed
v y-component of velocity
W half the width of the cast material, see Fig. 1
x, y spacial coordinates, see Fig. 1
x^*, y^* non-dimensional spacial coordinates, x/W, y/W.

Greek symbols

α thermal diffusivity, $k/\rho C$
β coefficient of volumetric expansion
ε emissivity
Θ dimensionless temperature, $(T-T_\infty)/(T_f-T_\infty)$
Θ_o superheat, $(T_o-T_\infty)/(T_f-T_\infty)$
μ dynamic viscosity
ρ density
σ Stefan–Boltzmann constant.

Subscripts

f phase change
l liquidus or liquid
m mold
o inlet
s solidus or solid
∞ ambient.

1. Introduction

There has been a growing research interest in the melting and solidification technology among mathematicians

* Corresponding author. Tel.: +1-406-994-6295; fax: +1-406-994-6292; e-mail: ramin@me.montana.edu

0017–9310/99/$ - see front matter
PII: S0017–9310(98)00366–4

and engineers. The topic has obvious practical importance in a wide range of applications. The heat transfer and fluid flow mechanisms involving phase change are of sufficient complexity due to the nonlinear nature of the governing equations. Several analytical techniques have been developed for solid–liquid phase change problems. These include: heat balance integral method [1], variation technique [2], embedding method [3], isotherm migration method [4], source and sink method [5], and Cauchy boundary value method [6]. Analytical methods provide approximate solutions and have a common drawback. They result in very complicated mathematical formulations when solving multidimensional problems and sometimes become impossible to solve without oversimplification. Phase change problems involving melting or solidification are referred to as free boundary or moving boundary problems. The solution of this type of problem is inherently difficult, because at the solid–liquid interface, there is a discontinuity in the temperature gradient (heat flux) due to the liberation or absorption of energy (latent heat). Therefore, the solid–liquid interface moves with time, the location of which is not known a priori; it must be followed as part of the solution process.

A basic continuous casting process is shown in Fig. 1. It involves two steps. The molten metal first passes through a mold, which is usually cooled by water, followed by a high cooling rate at downstream. Consequently, the molten metal solidifies and the solidified ingot is withdrawn at a uniform velocity. This process is also similar to some other manufacturing techniques like optical and glass fiber drawing, wire drawing, hot rolling, plastic extrusion and Czochralski crystal growing. A close relationship exists between the mechanical behavior of polycrystalline metallic materials (i.e., castings, ingots, etc.) and their microstructural soundness. The structural perfection of a casting or ingot depends on many parameters such as grain size and growth, temperature gradient at the solid–liquid interface, and the rate of thermal cooling. Interaction among these parameters is mainly controlled by the cooling rate. The heat extraction rate in a solidifying process, by different cooling methods, produces variations of microstructure as well as metallurgical and mechanical properties.

An earlier evaluation by Sparrow et al. [7] of the previous work in this area noted that most of the analyses assumed that conduction heat transfer was the only transport mechanism of significant importance. Obviously, such an assumption is not applicable in all problems. When the molten metal flows under an imposed pressure gradient, forced convective flow occurs. Similarly, buoyancy induced flow may occur in the molten metal pool due to non-uniform temperature distribution. Thus, for a large class of problems, the assumption of only conduction heat transfer is not valid; the influence of convective flow must also be considered in many phase change transport processes. The review paper by Viskanta [8] discusses the recent advances in the understanding of melting and solidification mechanisms in metals and alloys. The importance of the convective flows, in particular, the buoyancy induced flows, is discussed. Jaluria [9] reviewed the works on the transport mechanisms from continuously moving materials undergoing thermal processing.

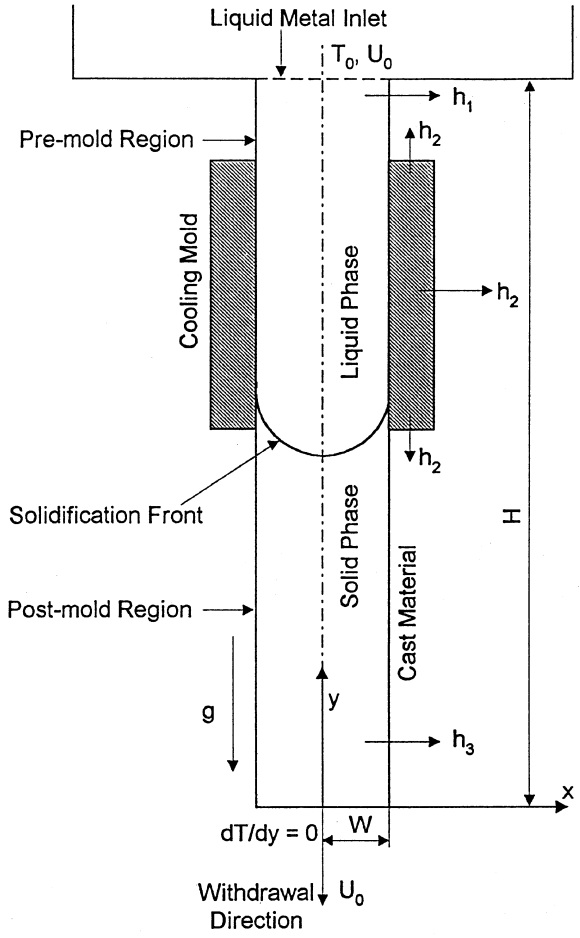

Fig. 1. Investigated geometry.

Investigators like Blackwell and Ockendon [10], Szekely et al. [11], DeBellis and LeBeau [12] have performed analytical and numerical studies on continuous casting problems. Since its inception, the so-called enthalpy model (single region approach) has been widely used to solve phase change problems. Bennon and Incropera [13] have used the enthalpy method to solve a solidification flow process in a channel. Among others, Chidiac et al. [14] have used enthalpy method in the transient continuous casting process.

A continuous casting process involves two distinct cooling mechanisms. Molten metal first flows through a

mold where cooling is done by circulating water through the mold. By the time the moving metal leaves the mold, depending on the cooling rate, the molten metal solidifies either completely or, at least, a solid crust develops on the outer periphery. Development of this solidified crust before leaving the mold region is very much essential to avoid a breakout and subsequent disaster of the process. Downstream, in the sub-mold region, the moving metal is cooled more rapidly by spray cooling. Roy Choudhury and Jaluria [15] performed a numerical study of the forced convection cooling of a continuously moving cylindrical rod. Both aiding and opposing flows of the cooling fluid were considered. The heat transfer in the mold region was not considered in their study. In another study, Kang and Jaluria [16] used enthalpy method to model the thermal phenomena in a continuous casting process. They considered the pre-mold, mold, and sub-mold regions in their study. Recently, Aboutalebi et al. [17] performed a numerical study of coupled turbulent flow and solidification for a continuously moving slab caster. Using enthalpy–porosity method, the authors considered both the mold and sub-mold regions.

It is seen from the preceding discussion that none of the studies has considered the effects of mold thickness and the conjugate heat transfer in the mold region for a continuous casting process. A recent study by Viswanath and Jaluria [18] on solidification in an enclosed region, shows the importance of considering the conjugate heat transfer in the mold region. Their study also shows the importance of considering the effects of mold thickness and aspect ratio. During solidification, most of the metals shrink. As a result, an air gap is created between the metal and mold. The heat transfer coefficient at this interface is nonlinear. Kim et al. [19], Huang et al. [20] and Piwonka and Berry [21] have done some exploration on the variable convective and radiative heat transfer at the metal–mold interface.

Following Bonacina et al. [22], Gartling [23] used an effective heat capacity method to solve transient phase change problems, using the finite element method. The advantage of this method is that a fixed grid can be used for the numerical computation. However, the limitation of this method is the selection of appropriate time step for the transient process. The time step should be chosen such that the temperature difference (between the solidus and liquidus temperature) progresses through the mesh without stepping over nodes (too high temperature difference) or falling completely between nodes (too low temperature difference). Hsiao [24] introduced an average heat capacity algorithm based on finite difference method where the limitation of time step was eliminated. Later, Lee and Chiou [25] modified this method for the finite element technique. In this research, Lee and Chiou's algorithm is used for the numerical computation. The radiation heat transfer at the metal–mold interface is taken into account. The conduction heat transfer effects in the mold and solidified metal were considered. Thus, the effects of the conjugate heat transfer were considered. Figure 1 shows the investigated geometry where different heat transfer rates were assigned in the pre-mold, mold and post-mold regions. Liquid metal enters the pre-mold at a constant inlet temperature and the solidified metal is withdrawn at a specified speed. Successful implementation of the average heat capacity method along with the conjugate heat transfer mechanism is achieved in this study.

2. Mathematical formulation

2.1. Governing equations

The geometry shown in Fig. 1 is used for the present study. The governing equations are simplified by the following assumptions: (i) the geometry is limited to two dimensions, (ii) the fluid is Newtonian, (iii) the flow is laminar, incompressible and within Boussinesq approximation, (iv) the change in material density upon the change of the phase is negligible, (v) the fluid is radiatively nonparticipating, (vi) the effects of latent heat will be adequately accounted for through appropriate modification of the specific heat, (vii) viscous dissipation and compressive work are negligibly small. Based on these assumptions, the conservation of mass, momentum, and energy equations in dimensional form can be written as

$$\frac{\partial u}{\partial x}+\frac{\partial v}{\partial y}=0 \tag{1}$$

Momentum equation in x- and y-directions respectively have the following forms:

$$\rho\frac{\partial u}{\partial t}+\rho u\frac{\partial u}{\partial x}+\rho v\frac{\partial u}{\partial y}=-\frac{\partial P}{\partial x}+\mu\left[\frac{\partial^2 u}{\partial x^2}+\frac{\partial^2 u}{\partial y^2}\right] \tag{2}$$

$$\rho\frac{\partial v}{\partial t}+\rho u\frac{\partial v}{\partial x}+\rho v\frac{\partial v}{\partial y} =-\frac{\partial P}{\partial y}+\mu\left[\frac{\partial^2 v}{\partial x^2}+\frac{\partial^2 v}{\partial y^2}\right]+\rho g\beta(T-T_\infty) \tag{3}$$

The energy equation is:

$$\rho C_{\mathrm{p}}\left[\frac{\partial T}{\partial t}+u\frac{\partial T}{\partial x}+v\frac{\partial T}{\partial y}\right]=k\left[\frac{\partial^2 T}{\partial x^2}+\frac{\partial^2 T}{\partial y^2}\right] \tag{4}$$

Density, ρ, is constant throughout the solid and liquid phases. Specific heat, C_{p}, is constant in liquid (C_{pl}) and solid (C_{ps}) phases. Specific heat in the solidification region is evaluated according to the average specific heat method to accommodate for the latent heat removal. The specific heat at a node undergoing phase change can be expressed as follows,

$$C_p(T_{i,j}) = \frac{1}{4}[C_{p1}(T_{i,j},T_{av,1}) + C_{p2}(T_{i,j},T_{av,2}) + C_{p3}(T_{i,j},T_{av,3}) + C_{p4}(T_{i,j},T_{av,4})] \quad (5)$$

$$T_{av,i} = \frac{1}{4}(T_{1n} + T_{2n} + T_{3n} + T_{4n}) \quad (6)$$

Here, $T_{av,i}$ is the average temperature of the ith adjacent sub-element. $C_p(T_{i,j}, T_{av,i})$ the adjusted specific heat [24], is a function of the latent heat (L), liquid specific heat (C_{pl}), and solid specific heat (C_{ps}). In equation (6), T_{1n}, T_{2n}, T_{3n}, and T_{4n} are the nodal temperatures of four-noded sub-elements. Details of this method are documented [24, 25]. The thermal conductivity, k, is defined as follows:

$$k = k_s \quad \text{for} \quad T < T_f - \Delta T$$

$$k = k_s + \frac{k_l - k_s}{2\Delta T}[T - (T - \Delta T)] \quad \text{for} \quad T_f - \Delta T \leqslant T \leqslant T_f + + \Delta T$$

$$k = k_l \quad \text{for} \quad T > T_f + \Delta T \quad (7)$$

where T_f is the solidification temperature and $2\Delta T$ is the small temperature difference across the solidification temperature, T_f.

In the continuity and momentum equations, liquid metal properties are used. When the temperature reaches the solidification temperature, T_f, a very high value of fluid viscosity is assigned to essentially solve a very stiff momentum equation. This process eliminates continuity and momentum equations when solidification is achieved. The only governing equation that controls the heat transfer process at that state is the energy equation. When solidification occurs, the velocity vector in the energy equation for the cast material is assigned a zero value for the x-component and the constant withdrawal speed, U_o, in the appropriate direction, for the y-component. The relevant boundary conditions for the above governing equations are shown in Fig. 1. The phase boundary conditions are also satisfied by the use of equations (5) and (7). This is the essence of the average heat capacity method, used in the present analysis.

Liquid metal shrinks upon solidification, resulting in an air gap between the mold and the solidified metal. The mold–metal interfacial heat transfer is taken into account by applying a radiative heat transfer coefficient at the interface.

$$h_r = \frac{\sigma(T_m^2 - T_s^2)(T_m + T_s)}{\frac{1}{\varepsilon_m} + \frac{1}{\varepsilon_s} - 1} \quad (8)$$

In the above equation, T_m and T_s are the temperatures of the mold surface and the solidified metal at a particular location, respectively. These temperatures change with time until steady state is reached.

In conjugate heat transfer problems, the continuity of temperature and heat flux at the liquid metal and the solid mold interface must be satisfied. This continuity at the liquid metal and the mold interface is termed as the boundary condition of the fourth kind. They are expressed by equating the heat flux of the liquid metal with the heat flux of the mold and by equating the temperature of the liquid metal with the temperature of the mold, at the interface. The present analysis was performed by using the finite element technique based on the Galerkin method of weighted residual (GMWR). Therefore, the boundary conditions of the fourth kind were naturally enforced through elemental surface integrals generated by the GMWR.

2.2. Heat transfer

The dimensionless local heat flux along the outside of the cast material is defined as

$$q^{*\prime\prime} = \frac{q'' H}{k(T - T_\infty)} \quad (9)$$

Here, q'', is the local heat flux in dimensional form. The thermal conductivity, k, in equation (9) is not constant throughout the domain. It assumes the appropriate values for solid or liquid and is constant for each phase. The dimensionless average heat flux, Q, for the outer surface is determined by integrating the local heat flux values as shown below.

$$Q = \int_0^1 q^{*\prime\prime}\, dy^* \quad (10)$$

Simpson's rule is used to perform the integration.

3. Numerical procedure

3.1. Code description

As a starting point, the finite element code NACHOS II, developed by Gartling [26] was used. It is a general-purpose finite element code designed to solve the two-dimensional continuity, momentum, and energy equations for both steady state and transient problems. A detail description of the code has been documented [26]. For the purpose of the present two-phase problem, substantial modification of code has been made to incorporate the average heat capacity method. The grids were generated by the internal grid generator of the code. The dimensional forms of the governing equations were solved. Results are obtained in terms of primitive variables. All computations were performed on a DEC Alpha 2100 machine.

3.2. Computational models

Due to the symmetry along the centerline, half of the geometry shown in Fig. 1 was used for the numerical computation. In order to set the required fluid flow and

heat transfer conditions using convenient parameters, the non-dimensional form of the governing equations and boundary conditions were used. The definitions of the various non-dimensional parameters used to set the conditions of the present problem are listed in the nomenclature section. The withdrawal speed is represented in non-dimensional form as the Peclet number (*Pe*). The difference between the inlet temperature of the liquid metal and the solidification temperature, known as the superheat, is expressed in non-dimensional form as Θ_o. Other important non-dimensional parameters are the Stefan number (*Ste*) and the Biot number (*Bi*). The length scale is non-dimensionalized by half of the casting width, *W*.

3.3. Grid independence test and code validation

In order to establish the accuracy of the results obtained by the present method, grid independence test was conducted first. Three different grid sizes were tested. After establishing the grid independence, 374 elements were chosen for the current geometry. Each element contained nine nodes, which resulted in 1617 nodes in total for the entire domain. More elements were packed in the areas of expected higher temperature and/or velocity gradients. Following the grid independence test, several cases were run to compare with the analytical results reported by Siegel [6]. Figure 2 shows the comparison of the results obtained by the current method with the analytical results. Good agreement can be seen. The details of the grid independence test and comparison with the analytical results are reported by Greif [27].

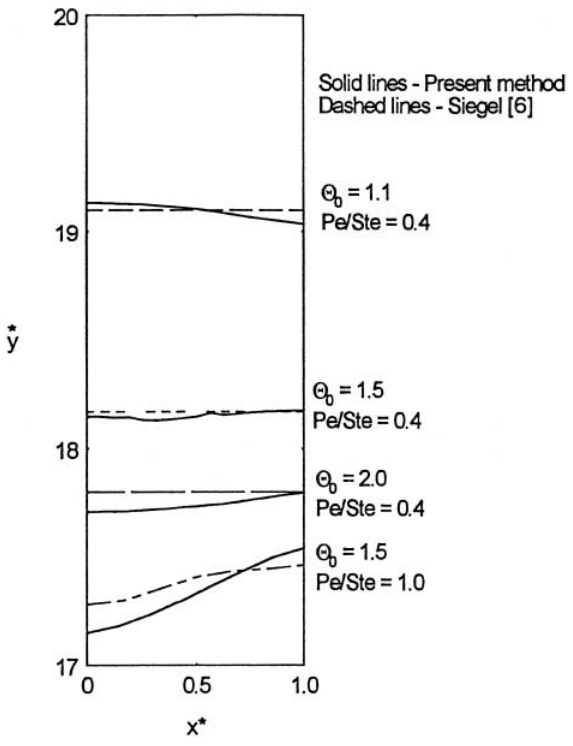

Fig. 2. Comparison with the analytical results of Siegel [6].

4. Results and discussion

As discussed before, the present research was conducted to evaluate the two-phase solidification process during a continuous casting process. The average specific heat method was successfully implemented in the numerical algorithm to balance the energy during the change of phase. Numerical exercise was performed to determine the effects of mold and post-mold cooling rates coupled with different withdrawal speeds and inlet temperatures of the molten metal. During a continuous casting process, one of the important aspects to consider is to avoid the breakout condition of the cast material. That is, if the liquid metal does not form a solid outer crust before leaving the mold region, a breakout will occur. This will lead to disaster and ultimate shutdown of the casting process.

For the purpose of generality, the results are presented in non-dimensional terms. Four parameters, namely, the mold cooling rate (Bi_2), post-mold cooling rate (Bi_3), amount of superheat (Θ_0) and withdrawal speed (*Pe*) were varied. The pre-mold region was assumed to be insulated ($Bi_1 = 0$) and a constant Stefan number (*Ste*) of 2.5 was used throughout this study. The ranges of other parameters used were $Pe = 1.0$–3.45, $\Theta_0 = 1.2$–2.7, $Bi_2 = 0.025$–0.075, $Bi_3 = 0.042$–0.126. An aspect ratio of 20 was used for the cast material. As reported by Kang and Jaluria [16], this aspect ratio is found to be adequate to obtain a developed temperature distribution. The pre-mold, mold, and post-mold non-dimensional distances used in the current research were 2, 8, and 10, respectively. A mold aspect ratio of 32 was used. Aluminum and copper are used as the cast and mold materials respectively.

Figure 3 shows the effects of withdrawal speed (*Pe*) on the location and shape of the solidification front for low cooling rates ($Bi_2 = 0.025$, $Bi_3 = 0.042$) and high cooling rates ($Bi_2 = 0.075$, $Bi_3 = 0.126$). As expected, it can be seen that with the increase of the withdrawal speed, the solidification front moves downstream. For low cooling rates (Fig. 3(a)), a breakout condition occurs when the *Pe* is increased above 2.0. As reported by Huang et al. [20], a maximum safe casting speed exists for a particular set of values for superheat and cooling rates. By comparing Fig. 3(a) and (b), we can see that for low cooling rates, the slope of the solidification front is much steeper. This is because with increased withdrawal speed, the fluid velocity increases and there is less time for heat extraction in the mold and post-mold regions. Hence, the gradient of the solidification front becomes steeper. For structural

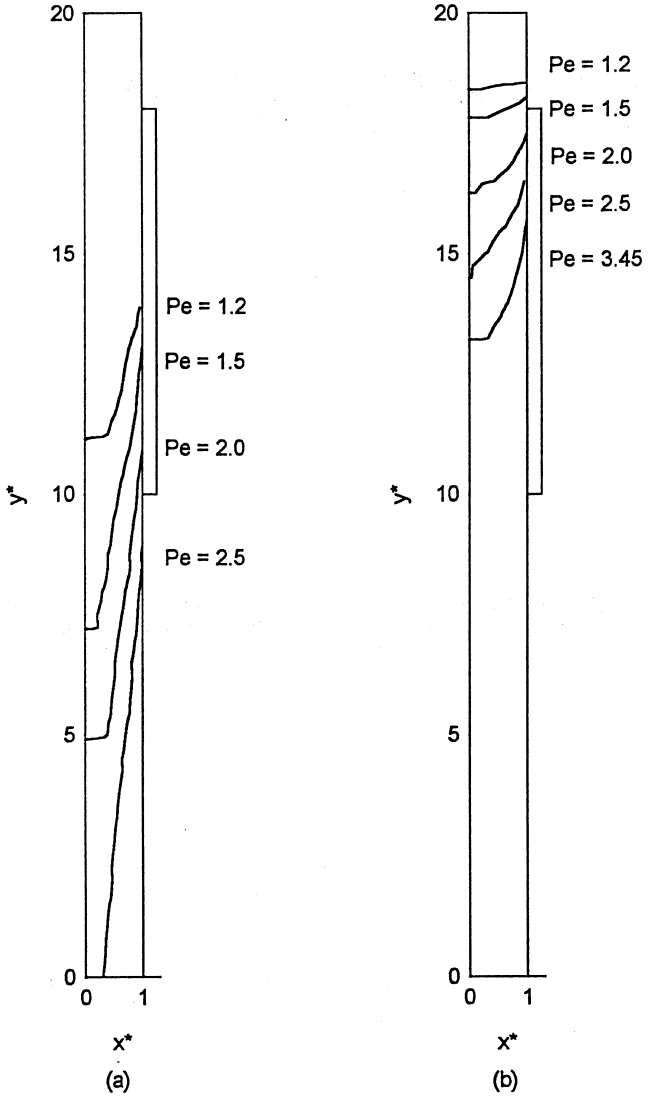

Fig. 3. Effects of withdrawal speed for (a) $\Theta_0 = 1.2$, $Bi_2 = 0.025$, $Bi_3 = 0.042$, (b) $\Theta_0 = 1.2$, $Bi_2 = 0.075$, $Bi_3 = 0.126$.

uniformity of the cast material, it is desired to have the solidification front slope as low as possible. From Fig. 3(a) and (b), it can be seen that for fixed values of Θ_o and *Pe*, the structural uniformity can be significantly improved by increasing the mold and post-mold cooling rates. For the high cooling rate cases, as shown in Fig. 3(b), it was not possible to achieve the limiting value of *Pe* at which the breakout occurs. The numerical solution became unstable beyond a value of $Pe = 3.45$.

Figure 4 shows the outside surface temperature of the cast material for different withdrawal speeds and for two different cooling rates. It can be seen that the temperature change in the pre-mold region ($y^* = 18$–20) is much smaller with the change of *Pe* when compared with the mold and post-mold regions. This is due to the fact that the pre-mold region is assumed insulated in this study. As such, the heat transfer in that region is in the axial direction only. It can also be seen by comparing Fig. 4(a) and (b) that at lower cooling rates, the change in pre-mold temperature distribution is very low with the change of *Pe*. In general, it can be seen from Fig. 4 that with the increase of withdrawal speed, the outside surface temperature of the cast material remains at a higher value. This is because of the fact that increased withdrawal speed constitutes higher amount of hot molten metal that needs to be cooled. As such, the solidification front moves downstream and hence higher temperature of the cast material. This situation can be improved by increasing the mold and post-mold cooling rates and can be seen by comparing the temperature values of Fig. 4(a) and (b).

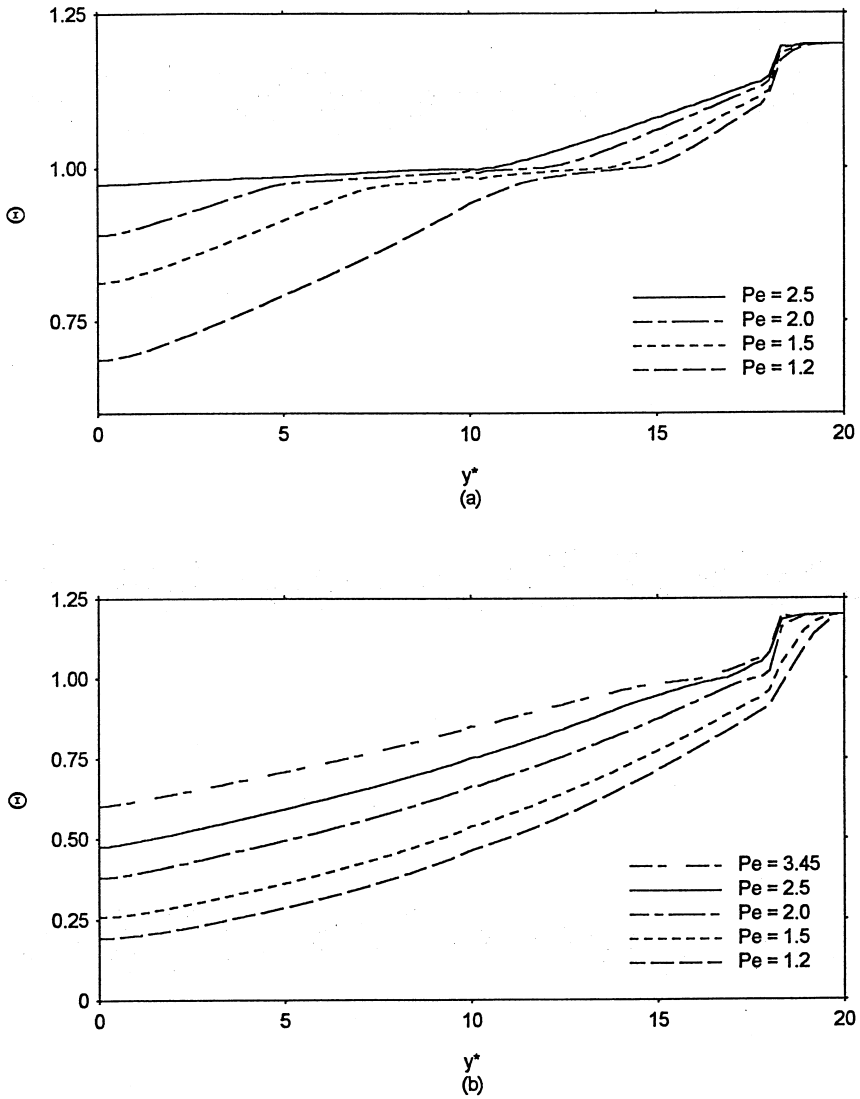

Fig. 4. Outside surface temperature for (a) $Bi_2 = 0.025$, $Bi_3 = 0.042$, (b) $Bi_2 = 0.075$, $Bi_3 = 0.126$.

Similar trends were observed for centerline temperature distribution of the cast material.

It is interesting to note from Fig. 4(a) that for lower cooling rates, a section of the temperature curve remains almost isothermal. This can be explained by comparing the locations of the solidification fronts for the same cases shown in Fig. 3(a). The constant temperature section of Fig. 4(a) (in y^*-direction) almost coincides with the section in Fig. 3(a) that marks the beginning and the end of the solidification front. With increased value of the withdrawal speed (Pe), the solidification front is stretched to a longer distance, Fig. 3(a), and so is the constant temperature section of Fig. 4(a). This observation verifies the fact that the temperature of the region undergoing phase-change remains constant due to latent heat absorption. From the presented results, this phenomenon is less prominent when the cooling rates are increased, Fig. 4(b).

The local non-dimensional heat flux values along the outer surface of the cast material were evaluated by using equation (9). Figure 5 shows the heat flux values for cases with $\Theta_o = 1.2$, $Bi_2 = 0.075$, $Bi_3 = 0.126$, $Pe = 1.2$–3.45. It can be seen that with the increase of the withdrawal speed, the local heat transfer rate along the surface increases. This is because with the increase of the withdrawal speed, the amount of hot molten metal flow increases and hence the increased amount of heat transfer. This observation is consistent with the solidification front location and the surface temperatures for different withdrawal speeds as shown in Figs 3(b) and 4(b) respectively. Figures 3 and 4 show that with the increase of

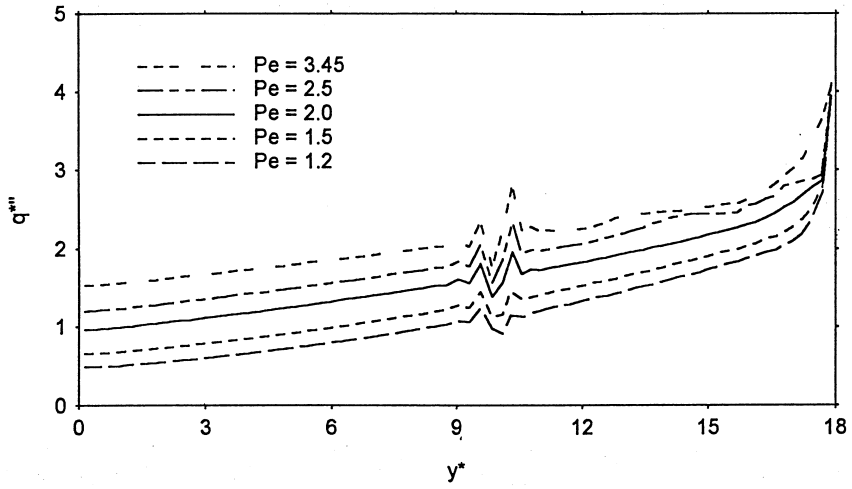

Fig. 5. Effects of withdrawal speed on local heat flux for $\Theta_0 = 1.2$, $Bi_2 = 0.075$, $Bi_3 = 0.126$.

Pe, the solidification front moves downstream and the surface temperature increases. The discontinuity of the curves in Fig. 5 at $y^* = 10$ is due to the change of cooling rate in the mold and post-mold regions. Due to the higher temperature in mold region, the heat transfer rate is also higher there. The local heat flux values were numerically integrated to obtain the average non-dimensional heat flux values (Q) for different withdrawal speeds (Pe). As expected, the average heat transfer rate increases with the increase of the Pe. Equation (11) shows the correlation for the average heat flux, Q, with the withdrawal speed, Pe. The ranges of parameters for this correlation are $\Theta_o = 1.2$, $Bi_2 = 0.075$, $Bi_3 = 0.126$, $Pe = 1.0$–3.45.

$$Q = 17.7 \cdot Pe^{0.754} \tag{11}$$

The inlet temperature of the molten material determines the amount of heat that must be removed before solidification can occur. Therefore, it is an important parameter in metal casting and is usually expressed as the difference of the inlet molten metal temperature and the solidification temperature, called the superheat. Figure 6 shows the locations of the solidification fronts for different values of the non-dimensional superheat, Θ_o. Two different withdrawal speeds, $Pe = 1.5$ and 2.5 were used. The mold and post-mold cooling rates are $Bi_2 = 0.075$, $Bi_3 = 0.126$, respectively. As expected, with the increase of superheat, the solidification front moves downstream. The figure shows that for higher values of Pe, the breakout condition occurs at a lower value of superheat. As discussed before, the shape of the solidification front is very much crucial in controlling the structural uniformity of the cast material. A steeper solidification front results in higher structural non-uniformity. It can be seen from Fig. 6 that the shape of the solidification front remains almost unchanged with the change of the amount of superheat. An inspection of the heat transfer rate from the cast material revealed that for constant values of Bi_2 and Bi_3, the percentage of the heat removed by the mold region remains the same with the increase of the superheat, Θ_o. Similar observation was made by Huang et al. [20]. A correlation was developed for the average heat flux, Q, as a function of the superheat, Θ_o, and is shown in equation (12). The ranges of parameters for this equation are $Pe = 1.5$, $Bi_2 = 0.075$, $Bi_3 = 0.126$, and $\Theta_o = 1.2$–2.7.

$$Q = 18.1\Theta_o^{1.71} \tag{12}$$

Cooling rates in the mold and post-mold regions have a direct and significant effect on the solidification process. The rate of cooling affects the location of the solidification front, total heat flux, the temperature profiles and hence the physical properties and microstructure of the solidified material. In this research, it was observed that two parameters, namely, Pe and Θ_o have significant effect on the quality of the cast product. These two parameters play a vital role to determine the breakout condition during a continuous casting process. Figure 7 shows the solidification front locations for different values of mold cooling rate, Bi_2. The other parameters used for this figure were $Pe = 2.5$, $\Theta_o = 1.2$, and $Bi_3 = 0.126$. It can be seen that with the increase of the mold cooling rate, the solidification front moves upstream and the slope of the front becomes steeper. At lower values of the mold cooling rate, the solidification front slope decreases significantly. This trend of the solidification front slope is different from the cases when mold and post-mold cooling rates are increased at the same time while keeping the values of Pe and Θ_o constant (Fig. 3). The microstructure of the cast product is dendritic, more dense and uniform, when the material undergoes the same treatment throughout the mold

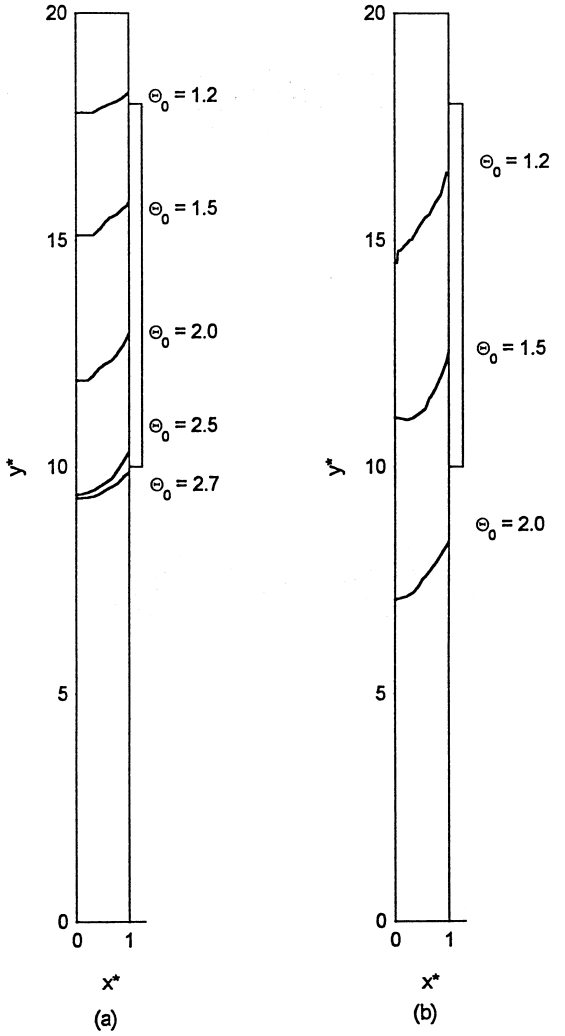

Fig. 6. Effects of superheat on solidification front position for $Bi_2 = 0.075$, $Bi_3 = 0.126$; (a) $Pe = 1.5$, (b) $Pe = 2.5$.

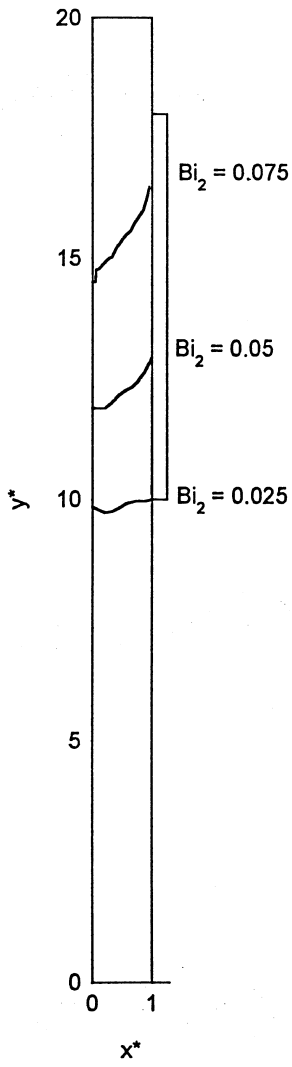

Fig. 7. Effects of the mold cooling rate on solidification front position for $Pe = 2.5$, $\Theta_o = 1.2$, $Bi_3 = 0.126$.

region. The material becomes less dense and non-uniform when the interface slope becomes steep.

It can also be seen from Fig. 7 that at lower values of mold cooling, the breakout condition approaches faster. It is discussed previously that the withdrawal speed also affects the solidification front slope and the breakout condition. Lower values of withdrawal speed decrease productivity and higher values of cooling rate increase the production cost. Therefore, a cost-effective combination between these parameters is very much desired. From Fig. 7, it can be concluded that for a set of casting conditions, that is, Pe, Θ_o, and Bi_3, a minimum value of Bi_2 exists beyond which the breakout condition will occur.

Figure 8 shows the local heat flux values on the outer surface of the cast material for different mold cooling rates with $Pe = 1.2$, $\Theta_o = 1.2$, and $Bi_3 = 0.126$. An interesting feature of this figure is that for lower mold cooling rates ($Bi_2 = 0.025$, 0.05), more heat is being extracted from the post-mold region ($y^* = 0$–10). Otherwise, in general, it is observed to have more heat extraction in the mold region ($y^* = 10$–18) in comparison to the post-mold region. The percentage of the total heat transfer from the mold region was evaluated for different cooling rates and withdrawal speeds. It was observed that the for a fixed set of values of mold and post-mold cooling rates (Bi_2, Bi_3), the percentage of total heat transfer from the mold region remains almost the same for different values of Pe. As expected, the surface temperature of the cast material increases with the decrease of the cooling rate.

Figures 9 and 10 show the non-dimensional isotherms

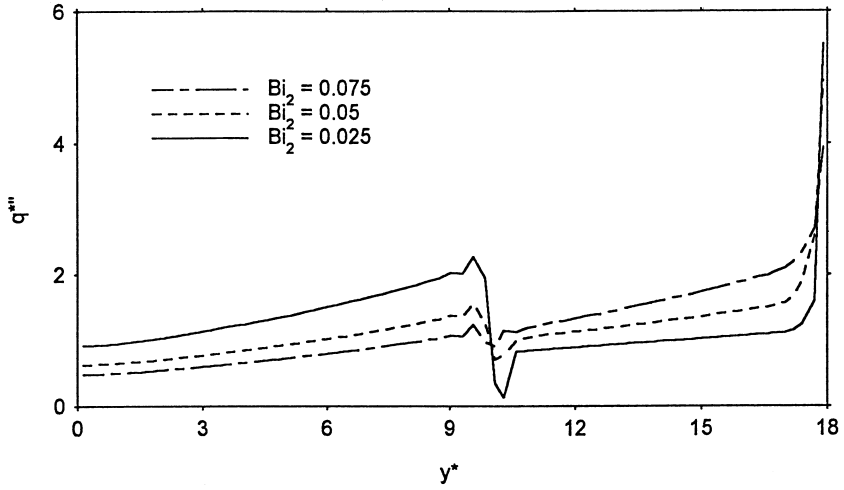

Fig. 8. Effects of mold cooling rate on local heat flux for $Pe = 1.2$, $\Theta_o = 1.2$, $Bi_3 = 0.126$.

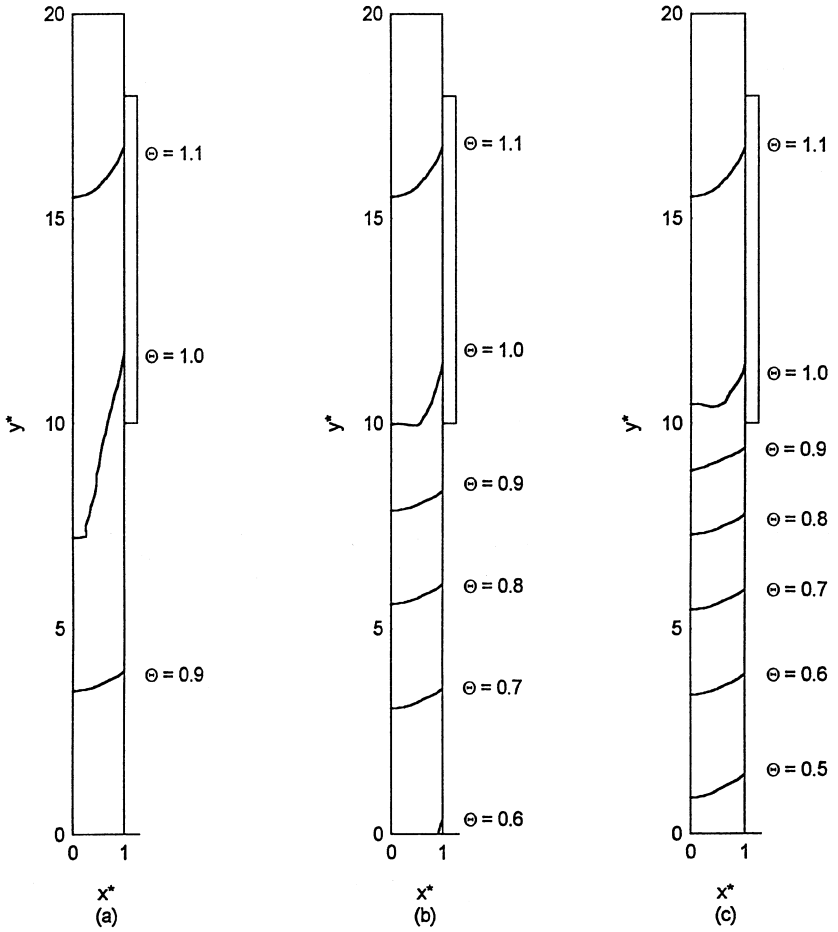

Fig. 9. Effects of post-mold cooling rate for $Pe = 1.5$, $\Theta_o = 1.2$, $Bi_2 = 0.025$; (a) $Bi_3 = 0.042$, (b) $Bi_3 = 0.084$, (c) $Bi_3 = 0.126$.

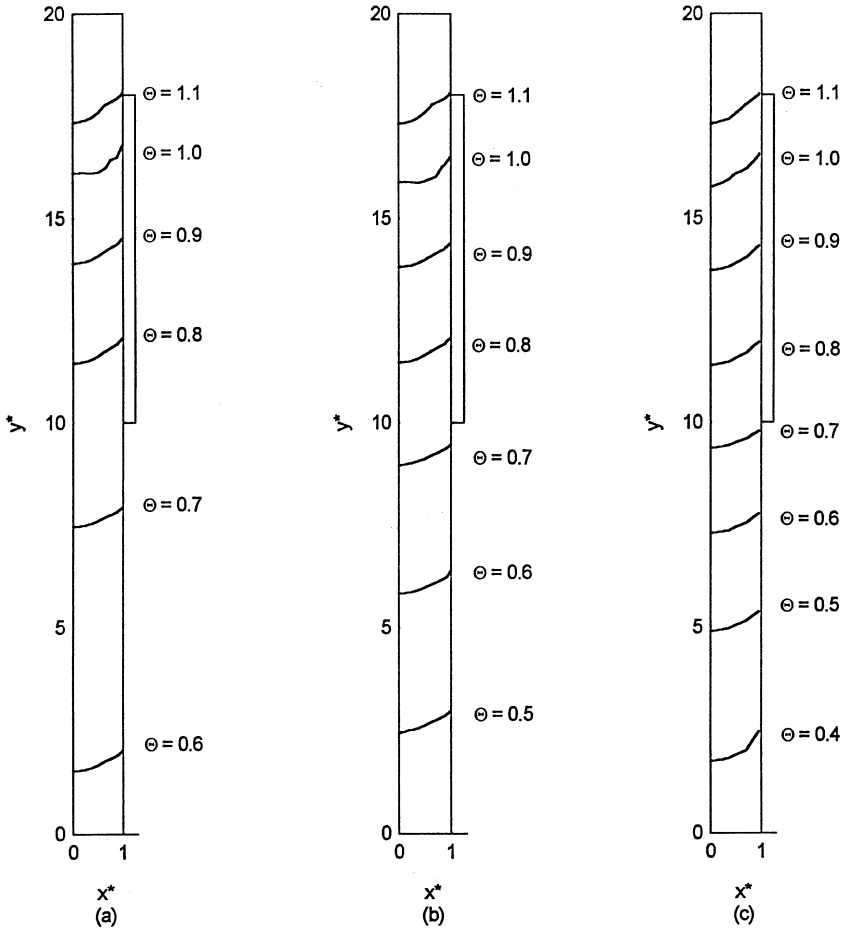

Fig. 10. Effects of post-mold cooling rate for $Pe = 1.5$, $\Theta_o = 1.2$, $Bi_2 = 0.05$; (a) $Bi_3 = 0.042$, (b) $Bi_3 = 0.084$, (c) $Bi_3 = 0.126$.

for the cast material with mold cooling rate $Bi_2 = 0.025$ and 0.05 respectively. The withdrawal speed (Pe) and superheat (Θ_o) were kept constant at 1.5 and 1.2, respectively. For each figure, the values of the post-mold cooling rate (Bi_3) were 0.042, 0.084 and 0.126. As expected, it can be seen from the figures that the post-mold temperature distribution changes with the post-mold cooling rate. However, the change of the post-mold cooling rate has little or no effect on the temperature distribution in the mold region. The location of the solidification front ($\Theta = 1.0$) also remains unaltered although its shape changes to some extent for some cases. By comparing Figs 9 and 10, we can see that the solidification front moves upstream with the increase of the mold cooling rate (Bi_2). This is consistent with the observation discussed earlier regarding Fig. 7.

An interesting feature is worth mentioning here. From Fig. 9(a), we can see that the solidification front ($\Theta = 1.0$) is stretched from the mold to the post-mold region. When the post-mold cooling rate is increased, keeping the mold cooling rate the same, the location of the solidification front in the mold region remains unaltered. However, the portion of the front in the post-mold region moves upstream with the increase of the post-mold cooling rate, and can be seen by comparing Fig. 9(b) and (c). An inspection of the surface temperature distribution of the cast material (not shown here) reveals that for a fixed value of Bi_2, the surface temperature distribution in the mold region does not change with the change of post-mold cooling rate. On the other hand, the surface temperature in the post-mold region decreases with the increase of the post-mold cooling rate (Bi_3). The local heat flux values along the cast material surface show similar trends. This is consistent with the isotherm distributions of Figs 9 and 10. That is, the isotherm locations in the mold region remain unaltered and the isotherm locations in the post-mold region change with the change of post-mold cooling rate.

It is discussed earlier that in this study, when the liquid metal solidifies, a radiation boundary condition is

imposed at the interface of the solidified metal and the mold. Inspection of the local temperature distribution at the interface revealed that for the ranges of parameters used in the current study, the temperature difference between the inside of mold surface and the solidified metal turned out to be very small. As such, no significant effect of radiation boundary condition at the interface was observed. One of the reasons for this insignificant effect could be the way the radiation boundary condition was imposed at the interface. In reality, when the liquid metal at the mold-metal interface solidifies, it shrinks and produces an air gap in between the two surfaces. This air gap in turn exerts a thermal resistance in addition to the radiation boundary condition. The absence of such resistance due to the air gap in the current method might be the reason for such insignificant change of the temperature values at the solidified metal–mold interface. Future analysis in 2D cylindrical coordinates might also give a more realistic solution. Therefore, further investigation on these issues is warranted.

5. Conclusions

The average heat capacity method using the finite element technique was successfully used to solve the two-phase solidification process in continuous castings. The main advantage of this method is that it overcomes the tedious requirement of changing the grid position for typical phase change problems. This method also overcomes the limitation of selecting and maintaining the appropriate time increment as required by the so-called effective heat capacity method [22]. Therefore, computational complexity is reduced by the current method. Good agreement with the results from other analytical method was obtained. The current method can also be successfully used in other phase change problems with moving materials.

It was observed in the current study that the withdrawal speed has a significant effect on the solidification process. It controls the solidification front location and shape, which directly contribute to the microstructural quality of the cast material and the determination of the breakout condition. The solidification front moves downstream and becomes steeper with the increase of the withdrawal speed. The withdrawal speed also has a strong effect on temperature distribution throughout the cast material and eventually resulted in controlling the heat extraction rate. The current research shows that the amount of superheat has a strong effect on the position of the solidification front, but it does not control the slope of the solidification front. This concludes that the amount of superheat is important to determine the breakout condition but not the quality of the cast material. Two correlations were developed for the average heat transfer rate from the cast material as functions of withdrawal speed and superheat respectively.

It was concluded in this study that the mold cooling rate is an important parameter to control the cast material microstructure and prevention of breakout condition. With the decrease of the mold cooling rate and withdrawal speed, the slope of the solidification front decreases. It was also observed in this study that for fixed values of superheat and withdrawal speed, the solidification front slope decreases significantly when the mold and post-mold cooling rates are increased (Fig. 3). The decreased slope of the front indicates improved microstructural quality of the cast material. On the other hand, the location and the slope of the solidification front were not found to be dependent on the post-mold cooling rates alone unless the solidification occurs very close to the end of the mold region. However, the post-mold cooling rate strongly influences the temperature distribution and heat transfer rate in that region. For a particular set of casting conditions, namely, withdrawal speed, superheat, and post-mold cooling rate, a minimum value of mold cooling rate is required to avoid the breakout condition.

Acknowledgements

This research was partially supported by a grant from MONTS, the NSF-EPSCoR program at Montana State University. The financial support from the MONTS program is greatly appreciated.

References

[1] T.R. Goodman, The heat balance integral and its application to problems involving a change of phase, Trans. ASME 80, (1958) 335–342.
[2] L.T. Yeh, B.T.F. Chung, Solidification and melting of material subjected to convection and radiation, J. Spacecr. Rockets 12, (1975) 329–334.
[3] B.A. Boley, The embedding technique in melting and solidification problems, in: J. Ockendon, W. Hodgins (Eds.), Moving Boundary Problems in Heat Flow and Diffusion, Proceedings of the Conference held at the University of Oxford, March, 1974, pp. 150–172.
[4] J. Crank, R. Gupta, Isotherm migration method in two dimensions, Int. J. Heat Mass Transfer 18 (1975) 1101–1117.
[5] S.C. Keung, The use of sources and sinks in solving two-dimensional heat conduction problems with change of phase in arbitrary domains, Ph.D. dissertation, Columbia University, New York, 1980.
[6] R. Siegel, Two-region analysis of interface shape in continuous casting with superheated liquid, J. Heat Transfer 106 (1984) 506–511.
[7] E.M. Sparrow, S.V. Patankar, S. Ramadhyani, Analysis of

melting in the presence of natural convection in the melt region, J. Heat Transfer 99 (1977) 520–526.
[8] R. Viskanta, Heat transfer during melting and solidification of metals, J. Heat Transfer 110 (1988) 1205–1219.
[9] Y. Jaluria, Transport from continuously moving materials undergoing thermal processing, Annual Review on Heat Transfer 4 (1992) 187–245.
[10] J.H. Blackwell, J.R. Ockendon, Exact solution of a Stefan problem relevant to continuous casting, Int. J. Heat Mass Transfer 25 (7) (1982) 1059–1060.
[11] J. Szekely, J.W. Evans, J.K. Brimacombe, Modeling of the continuous casting of steel, The Mathematical and Physical Modeling of Primary Metals Processing Operations, Wiley-Interscience, New York, 1988, Chap. 7, pp. 197–227.
[12] C.L. DeBellis, S.E. LeBeau, A verified thermal model for continuous casting process, in: R.K. Shah (Ed.), Heat Transfer in Manufacturing and Materials Processing, ASME 1989 National Heat Transfer Conference, NY, 1989, pp. 105–111.
[13] W.D. Bennon, F.P. Incropera, A continuum model for momentum, heat and species transport in binary solid–liquid phase change systems—I: model formulation, Int. J. Heat Mass Transfer 30 (10) (1987) 2161–2170.
[14] S.E. Chidiac, I.V. Samarasekera, J.K. Brimacombe, A numerical method for analysis of phase change in the continuous casting process, in: E.C. Thompson, R.D. Wood, O.C. Zienkiewick, A. Samuelson, A.A. Balkema (Eds.), Proceedings of Numiform 89, The Netherlands, 1989, pp. 121–128.
[15] S. Roy Choudhury, Y. Jaluria, Forced convective heat transfer from a continuously moving heated cylindrical rod in materials processing, J. Heat Transfer 116 (1994) 724–734.
[16] B.H. Kang, Y. Jaluria, Thermal modeling of the continuous casting process, J. Thermophysics and Heat Transfer 7 (1) (1993) 139–147.
[17] M.R. Aboutalebi, M. Hasan, R.I.L. Guthrie, Numerical study of coupled turbulent flow and solidification for steel slab casters, Numerical Heat Transfer, Part A 28 (1995) 279–297.
[18] R. Viswanath, Y. Jaluria, Numerical study of conjugate transient solidification in an enclosed region, Numerical Heat Transfer, Part A 27 (1995) 519–536.
[19] W.S. Kim, M.N. Ozisik, L.G Hector Jr., Inverse problem of 1D solidification for determining air-gap resistance to heat flow during metal casting, XXII ICHMT International Symposium on Manufacturing and Material Processing, Dubrovnik, Yugoslavia, 1990.
[20] C.H. Huang, M.N. Ozisik, B. Sawaf, Conjugate gradient method for determining unknown contact conductance during metal casting, Int. J. Heat Mass Transfer 35 (1992) 1779–1786.
[21] T.S. Piwonka, J.T. Berry, Heat transfer at the mold/metal interface in investment castings, Proceedings of the 41st Annual Technical Meeting—Investment Casting Institute, 1993, pp. 15:1–15:17.
[22] C. Bonacina, G. Comini, A. Fasano, and M. Primicerio, Numerical solution of phase-change problems, Int. J. Heat Mass Transfer 16 (1973) 1825–1832.
[23] D.K. Gartling, Finite element analysis of convective heat transfer problems with change of phase, in: K. Morgan, C. Taylor, C. Brebbia (Eds.), Computer Methods in Fluids, Pentech Press, U.K., 1980, pp. 257–284.
[24] J.S. Hsiao, An efficient algorithm for finite-difference analyses of heat transfer with melting and solidification, Numerical Heat Transfer 8 (1985) 653–666.
[25] R.-T. Lee, W.-Y. Chiou, Finite-element analysis of phase-change problems using multilevel techniques, Numerical Heat Transfer, Part B 27 (1995) 277–290.
[26] D.K. Gartling, NACHOS II—A Finite Element Computer Program for Incompressible Flow Problems, Part I—Theoretical Background, SAND86-1816, UC-32, Sandia Laboratories, Albuquerque, New Mexico, 1987.
[27] D. Greif, Numerical study of conjugate heat transfer in a continuously moving metal during solidification, M.S. Thesis, Montana State University, Bozeman, MT, 1998.